Journal of Applied Fluid Mechanics, Vol. 17, No. 9, pp. 1981-1992, 2024.
Available online at www.jafmonline.net, ISSN 1735-3572, EISSN 1735-3645.
https://doi.org/10.47176/jafm.17.9.2349

Effect of Spherical Silver Particles Size of the Catalyst Bed on Hydrogen Peroxide Monopropellant Thruster Performance

F. Benzenine [1†], C. Seladji [1], D. Darfilal [2] and O. Bendermel [1]

[1] *Department of Mechanical Engineering, Energetic and Applied Thermal Laboratory ETAP, University of technology, Chetouane 13000, Tlemcen, Algeria*
[2] *Satellites Development Center, Algerian Space Agency ASAL, IbnRochd USTO 31130, Oran, Algeria*

†Corresponding Author Email: fadela.benzenine@univ-tlemcen.dz

ABSTRACT

In this paper, an analytical approach combined with a two-dimensional computational fluid dynamics (CFD) model is pursued to simulate the fluid flow in a monopropellant thruster for satellite propulsion systems. The thruster utilizes hydrogen peroxide (H_2O_2) as a green propellant at a concentration of 87.5%, with a catalytic bed based on spherical silver particles. Through a parametric analysis of particle diameter, we aim to optimize the design of a monopropellant thruster capable of generating a thrust of 20N. For this purpose, a program in CFD code in the commercially available ANSYS Fluent software is used to solve the energy, momentum, mass transfer, and species transport equations governing the thruster system. The local thermal non-equilibrium (LTNE) approach is used to describe the heat transfer occurring through both the solid and fluid phases within the catalyst bed. The results demonstrate that particle size significantly affects the thermal behaviour, species mass fraction, and exit velocity. An optimum diameter of 0.65mm exhibits the optimal performance of the monopropellant thruster, ensuring efficient decomposition of H_2O_2 at 968K and providing the required level of thrust force with a specific impulse of about 120s.

Article History

Received September 29, 2023
Revised March 23, 2024
Accepted March 26, 2024
Available online July 2, 2024

Keywords:

Propulsion
Monopropellant thruster
Hydrogen peroxide
Catalyst packed-bed
Porous medium

1. INTRODUCTION

Monopropellant thruster (MPT) systems are widely used as propulsion systems in space applications, serving purposes such as spacecraft attitude control, orbit correction, and satellite manoeuvring, primarily due to their high reliability and simplicity (Hwang et al., 2012). These systems rely on a single substance that undergoes decomposition in a catalytic bed, creating a reaction that releases thermal energy and generates thrust force. Many MPT systems have utilized hydrazine as a propellant due to its high-performance capabilities. However, using hydrazine presents challenges as it is highly toxic, environmentally unfriendly, and costly during operations (Amri et al., 2013).

Numerous research studies have investigated the development of new propulsion systems using green propellants. These green propellants should be non-toxic and easy to handle and should offer relatively high performance at a lower cost, making them favourable for future missions in the space industry (Gibbon et al., 2001; Coxhill, 2002; Amri et al., 2013; Soejimaet al., 2016). A promising alternative involves using hydrogen peroxide (H_2O_2), also known as high-test peroxide (HTP), as a green propellant. H_2O_2 is considered relatively safe for both the environment and human handling (Chan et al., 2013).

For over 70 years, hydrogen peroxide has served as both a monopropellant and an oxidant (Lee & Lee, 2009). Its early use was documented by Walter (1956) in Germany, with applications in underwater vehicle propulsion systems and turbine pump drive systems. It subsequently became popular in high concentrations (>80%) for space propulsion applications. In the United Kingdom, extensive research focused on hydrogen peroxide, particularly for rocket-assisted launch engines designed for fast ascent and short runways (Sippel et al., 2011). Russia relies on hydrogen peroxide in the reaction control system (RCS) thrusters used during the descent stage of the Soyuz spacecraft, as well as for the gas generators that operate the turbine pumps (George, 2003). Similarly, in the United States, NASA laboratories extensively investigated the decomposition of hydrogen peroxide and its application in monopropellant rocket

NOMENCLATURE

A	section area	Re	Reynolds number
A_{fs}	interfacial area density	R_i	species production rate
C_2	inertial resistance factor	Y_i	local mass fraction of the species
C_p	specific heat	S_i	enthalpy Source term
d_p	particle diameter	T	temperature
D	diameter	T_0	inlet Temperature of H_2O_2
$D_{i,m}$	mass diffusion coefficient of the species	t	time
E_f	total energy	V	velocity
F_T	thrust Force	**Greek symbols**	
g	gravity	α	permeability
h	heat transfer coefficient	ε	porosity
h_{fs}	heat transfer coefficient between fluid and solid	μ	viscosity of the fluid
h_i	enthalpy of the species	γ	specific heat ratio
I	unit tensor	$\vec{v}$	velocity vector
I_{sp}	specific impulse	ρ	density
J_i	diffusion flux of the species	$\bar{\bar{\tau}}$	turbulent stress tensor
L	length	ω	specific dissipation
L_f	loading factor	**Subscripts**	
k	thermal conductivity	e	exit
k_{eff}	thermal conductivity effective	c	catalyst bed
$\dot{m}$	masse flow rate	f	refers to fluid
M	molar mass	i	injector
M_e	Mach number	S	refers to solid medium
P	pressure	t	throat
Pr	Prandtl number	T	tank
r	specific constant of perfect gases		

engines for the Mercury project spacecraft (Musker et al., 2006; Pasini et al., 2008). Recently, significant efforts have been directed towards developing new hydrogen peroxide monopropellant thrusters for the space industry, especially for future satellite applications (An et al., 2010; Amri et al., 2013; Koopmans et al., 2014; Palmer, 2014; Ryan et al., 2020).

The most important technological challenge in developing hydrogen peroxide monopropellant thruster systems is creating an efficient, reliable, and durable catalyst bed. The catalyst bed is a critical component of the thrusters, responsible for delivering fast and consistent performance while preventing poisoning by stabilizers and impurities in the propellant. It should also withstand multiple thermal cycles and ideally operate without requiring preheating for optimal efficiency.

Extensive research has been conducted to address the decomposition of high-concentration hydrogen peroxide in catalyst beds. Of the various materials explored, metallic silver is widely used as a catalyst for H_2O_2 decomposition due to its various advantages, including high decomposition efficiency, compactness, and a straight forward manufacturing process. Although silver catalysts exhibit superior efficiency compared to other available catalytic materials, their relatively low melting point temperature of approximately 961.8°C (1234.95K) limits their use to hydrogen peroxide concentrations below 92% (Ventura & Wernimont, 2001). It is also available in various forms, such as screen mesh, pellets, composites, flakes, and honeycomb structure thrusters. To reduce costs, silver was used as a coating on another metal instead of using pure silver. However, this does not significantly affect the reaction rate, as the reaction occurs mainly at the interface layer. The development of hydrogen peroxide monopropellant thrusters is reported in the work of Amri et al. (2013) and Haq et al. (2017), who each developed the 1N-class thruster by using a silver screen mesh catalyst and HTP at concentrations of 89% and 90%, respectively. Cervone et al. (2006) and Pasini et al. (2008) developed and tested this technique for 5N and 25N monopropellant thrusters using 87.5% hydrogen peroxide with pure silver screen and ceramic pellets as a catalyst, coated with manganese oxide and alumina-deposited platinum (Pt/γ-Al_2O_3). Other works utilized silver screen as a catalyst in developing a 50N and a 20N monopropellant thruster using hydrogen peroxide at a concentration of 90% and 87.5%, respectively (Palmer, 2014; Muhammad et al., 2021). A 100mN monopropellant micro-thruster was developed and tested using 0.7g of silver flakes as a catalyst with 92% hydrogen peroxide (Kuan et al., 2007). Further, 0.85N monopropellant thrusters were developed by using a composite silver catalyst and 90% hydrogen peroxide. Adami et al. (2015) used the same catalyst with different hydrogen peroxide concentrations of 85-95% in the multidisciplinary design optimization of a monopropellant thrusters, employing a genetic algorithm (GA) and sequential quadratic programming (SQP) for producing a thrust force of about 19-230N. A honeycomb structure was used as a catalyst bed in H_2O_2 decomposition for a micro-propulsion of 1N (Krejci et al., 2011). Other catalysts have also been studied, as in the experimental validation of 1N monopropellant thrusters utilizing 87.5% HTP with two different catalysts, platinum-coated gamma alumina particles and cylindrical ceria pellets (Ryan et al., 2020). Additionally, some studies have experimented with divanadium

pentoxide, lead oxide, and ruthenium dioxide (Rusek, 1996; An & Kwon, 2009). Silver, however, is still regarded as one of the most efficient heterogeneous catalysts for hydrogen peroxide decomposition (Runckel et al., 1963; Morlan et al., 1999; Pędziwiatr et al., 2018).

The fluid flow within the catalyst bed is complex, and the most appropriate approach to approximating this flow is to model the region as a porous medium (Xue et al., 2020). Such a medium is a heterogeneous system consisting of a solid substrate with fluid-filled voids (Srivastava & Bhadauria, 2016). The porosity of the porous catalyst bed greatly influences the performance and accuracy of the monopropellant thruster, affecting factors such as the pressure drop across the catalyst bed, reaction temperature, exit velocity, and thrust. Hence, selecting the optimal porosity for the silver catalyst bed is paramount in hydrogen peroxide monopropellant thrusters (Muhammad et al., 2021).

The performance of monopropellant thrusters also depends on optimizing their components, such as the injector, catalyst bed (length and diameter), and nozzle geometry. These components have a significant impact on the efficiency of the thruster (Palmer, 2014). In a monopropellant thruster system, the propellant hydrogen peroxide is injected into the porous medium of the catalyst bed, where it instantaneously decomposes by an exothermic reaction into a mixture of superheated steam and oxygen gas, which expands through a convergent-divergent (CD) nozzle to produce thrust force. The chemical reaction proceeds as follows:

$$H_2O_{2(l)} \xrightarrow{catalyst\ bed} H_2O_{(g)} + \frac{1}{2}O_{2(g)} + \Delta H$$

This study aims to develop a catalyst-packed bed containing spherical silver particles as a porous medium for the decomposition of propellant hydrogen peroxide at a concentration of 87.5%, intended for the use in a monopropellant thruster capable of generating 20N of thrust. A parametric analysis will be conducted to identify the optimal parameters for the thruster.

The commercially available CFD simulation software ANSYS Fluent was used to solve the energy, continuity, momentum, and species transport equations. The local thermal non-equilibrium (LTNE) approach is widely used to model convective heat transfer in a porous medium and to study thermal interactions between fluid and solid phases. The kinetics of the chemical reactions were computed using user-defined functions (UDFs).

2. MONOPROPELLANT THRUSTER DESCRIPTION

The monopropellant thruster consists of a cylindrical catalyst bed chamber (internal diameter 21mm and length 68.1mm) containing silver spherical particles of uniform size as a porous medium with a diameter of 0.65mm, selected from the experimental study by Pasini et al. (2008). We chose a conical nozzle type for this study due to its technical and economic advantages. According to the literature, the divergence angle is 30°, giving a half-angle of about 15°, which is used in many thrusters for attitude control. As for the convergence of the half-angle,

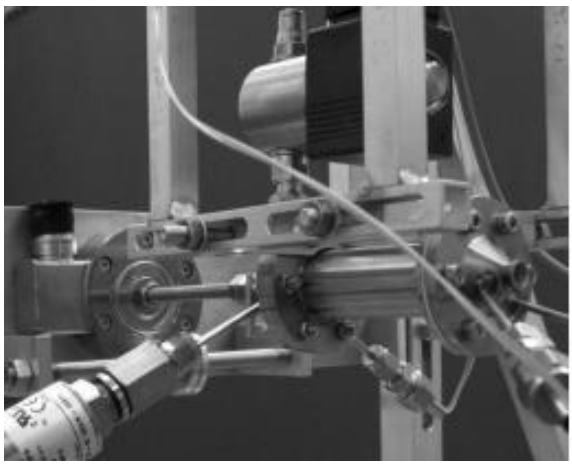

Fig. 1 Monopropellant thruster and load cell (Palmer, 2014)

a typical value of 60° is considered. The spray injector type chosen consisted of a hole with a diameter of 0.96637mm and a discharge coefficient of 0.7. We configured the 20N monopropellant thruster for sea-level conditions with a hydrogen peroxide feed pressure tank set at approximately 17bar with a mass flow rate of 17×10^{-3}kg/s. Further, 87.5% hydrogen peroxide with a density of 1378.5kg/m^3 at 20°C was selected, ensuring an extended catalyst life during thruster development (Vestnes, 2016). We used the parameters from Palmer's (2014) experimental work for the design model (Fig. 1). The thruster specifications are described in Table 1, while Fig. 2 depicts the thruster design with the proposed catalyst bed.

3. THEORETICAL AND COMPUTATIONAL MODELING

The study presents an approach for the computational modelling of a volumetric monopropellant thruster, which includes a cavity filled with a catalyst-packed bed containing silver spheres similar to a porous medium, an injector, and a nozzle. The simulation of flow physics and reactions within the thruster is based on mathematical models that account for the conservation of mass (the continuity equation), momentum, and energy.

3.1 Governing Equations

Equation (1) represents the conservation of mass law with additional isotropic porosity in a single-phase flow.

$$\frac{\partial \varepsilon\rho}{\partial t} + \nabla \cdot (\varepsilon\rho \vec{v}) = 0 \tag{1}$$

Table 1 Monopropellant thruster dimensions

Parameter	Value [mm]
Catalyst bed diameter D_c	21
Catalyst bed length L_c	68.1
Nozzle throat diameter D_t	4.3
Nozzle exit diameter D_e	6.5
Hole diameter D_i	0.96637
Injector length L_i	15

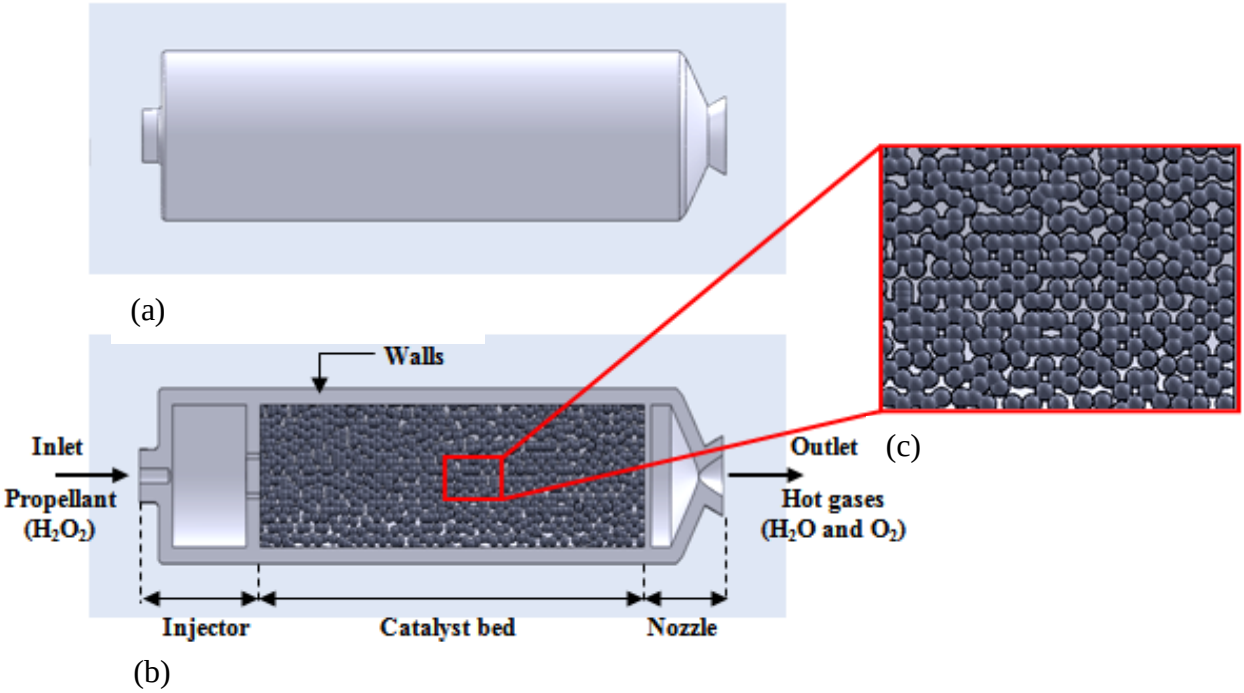

Fig. 2 (a) Full and (b) Sectional view of hydrogen peroxide monopropellant thruster design, and (c) spherical silver particles

where: ε is the porosity of catalyst bed, t is the time and $\vec{v}$ is the velocity vector.

Equation (2) represents the conservation of momentum. The turbulent stress tensor $\overline{\overline{\tau}}$ and the viscous loss term F, are defined in Eq. (3) and Eq. (4).

$$\frac{\partial}{\partial t}(\rho\vec{v})+\nabla\cdot(\rho\vec{v}\vec{v})=-\nabla p+\nabla\cdot\left(\overline{\overline{\tau}}\right)+\rho\vec{g}+F \tag{2}$$

$$\overline{\overline{\tau}}=\mu\left[\left(\nabla\vec{v}+\nabla\vec{v}^{T}\right)-\frac{2}{3}\nabla\cdot\vec{v}I\right] \tag{3}$$

$$F=-\left(\frac{\mu}{\alpha}v_i+C_2\frac{1}{2}\rho|v|v_i\right) \tag{4}$$

where: μ is the fluid viscosity and I is the unit tensor, α is permeability, $1/\alpha$ is the viscous resistance term and C_2 is inertial resistance.

For the energy equation in a porous medium, in the LTNE energy model approach, the fluid and solid phases are spatially identical and interact with each other in terms of heat transfer (Abdedou & Bouhadef, 2015). In the proposed model, two equations, Eq. (5) and Eq. (6), are solved separately for the fluid and solid phases, respectively, as follows:

$$\begin{aligned}&\frac{\partial}{\partial t}\left(\varepsilon\rho_f E_f\right)+\nabla\cdot\left(\vec{v}\left(\rho_f E_f+p\right)\right)=\\&\nabla\cdot\left(\varepsilon k_f\nabla T_f-\left(\sum_i h_i J_i\right)+\left(\overline{\overline{\tau}}\cdot\vec{v}\right)\right)\\&+S_f^h+h_{fs}A_{fs}\left(T_s-T_f\right)\end{aligned} \tag{5}$$

$$\begin{aligned}&\frac{\partial}{\partial t}\left((1-\varepsilon)\rho_S E_S\right)=\nabla\cdot\left((1-\varepsilon)k_S\nabla T_S\right)\\&+S_S^h+h_{fs}A_{fs}\left(T_f-T_S\right)\end{aligned} \tag{6}$$

where ρ_f and ρ_s are the densities of fluid and solid, T_f and T_s are temperatures of fluid and solids, k_f and k_s are the thermal conductivity of the fluid, ($\Sigma h_i J_i$) is the diffusion flux of the species is added when chemical reactions are considered, E_f and E_s are a total fluid and solid energy, S_f^h is the fluid enthalpy source term, h_{fs} present the convective volumetric heat transfer coefficient between the fluid and solid, and A_{fs} represent the interfacial area density, which is the ratio of the interfacial area of the fluid/solid and the volume of the porous medium.

Eq. (5) and Eq. (6) represent the source term of the convective heat exchange between the solid and the fluid phases due to the non-equilibrium thermal model by $h_{fs}\,A_{fs}\left(T_s-T_f\right)$ and $h_{fs}\,A_{fs}\left(T_f-T_s\right)$, respectively.

3.2 Convective Volumetric Heat Transfer Coefficient

According to Alazmi and Vafai, (2000) and Xu et al. (2011), the convective volumetric heat transfer coefficient is constant over the length of the porous medium. Table 2 provides an overview of some available models in the literature.

The convective volumetric heat transfer coefficient h_{fs} and the interfacial area density A_{fs} for a porous medium consisting of similarly sized spherical particles are calculated from Eq. (7) and Eq. (8), respectively (Vafai & Amiri, 1998).

Table 2 Different models of the volumetric heat transfer coefficient for porous medium

$h_{fs} = \overline{h_{fs}}$	A_{fs}	Reference
$\frac{k_f\left(2 + 1.1Pr^{1/3}Re^{0.6}\right)}{d_p}$	$\frac{6(1-\varepsilon)}{d_p}$	(Amiri & Vafai, 1994) (Amiri et al., 1995)
$\left[\frac{d_p\varepsilon}{0{,}2555Pr^{1/3}Re^{2/3}k_f} + \frac{d_p}{10k_s}\right]^{-1}$	$\frac{6(1-\varepsilon)}{d_p}$	(Dixon & Cresswell, 1979)
$\frac{((1.18Re^{0.58})^4 + (0.23Re_h^{0.75})^4)^{1/4}}{d_p k_f}$ where : $Re_h = \frac{Re}{1-\varepsilon}$	$\frac{6(1-\varepsilon)}{d_p}$	(Achenbach, 1995)
$0.004\left(\frac{d_v}{d_p}\right)\left(\frac{k_f}{d_p}\right)Pr^{0.33}Re^{1.35}$; $Re \le 75$ $1.064\left(\frac{k_f}{d_p}\right)Pr^{0.33}Re^{0.59}$; $Re \ge 350$	$\frac{20.346(1-\varepsilon)\varepsilon^2}{d_p}$	(Hwang et al., 1995)
$\left[2.096\varepsilon^{0.38}k_f Re^{0.438}(-8.278\varepsilon^{0.38} + 57.384\varepsilon^{1.38} - 106.63\varepsilon^{2.38} + 95.75\varepsilon^{3.38} - 37.24\varepsilon^{4.38})\right] / d_s^2$ for : $0.66 < \varepsilon < 0.93$ and $0.66 < Re < 0.93$	-	(Villafán et al., 2011)

$$h_{fs} = \frac{k_f\left(2 + 1.1\mathrm{Pr}^{\frac{1}{3}}\,\mathrm{Re}^{0.6}\right)}{d_p} \tag{7}$$

$$A_{fs} = \frac{6(1-\varepsilon)}{d_p} \tag{8}$$

where: d_p is the diameter of spherical silver particles, P_r is the Prandtl number and R_e is the Reynolds number.

3.3. Effective Conductivity

The effective thermal conductivity (k_{eff}) of a porous medium is generally calculated using correlations. This study used the more precise formulation of Kouichi (2008), which is the default model employed in ANSYS Fluent.

$$k_f = \varepsilon k_f \tag{9}$$

$$k_s = \frac{1}{3}(1-\varepsilon)k_s \tag{10}$$

$$k_{eff} = \varepsilon k_f + \frac{1}{3}(1-\varepsilon)k_s \tag{11}$$

3.4. Chemical Reactions Modeling

The chemical reaction conservation equation for the local mass fraction of the transport of each species, according to convective diffusion in a laminar flow within a catalyst bed (porous medium), is expressed as follows:

$$\frac{\partial}{\partial t}\left(\rho Y_i\right) + \nabla\cdot\left(\rho\vec{v}Y_i\right) = \nabla\cdot\left(\rho D_{i,m}\nabla Y_i\right) + R_i + S_i \tag{12}$$

Where: Y_i represents the local mass fraction of the species i, $D_{i,m}$ is the mass diffusion coefficient for the species i, R_i is the production rate in chemical reaction, and S_i is the rate of creation.

3.5. Permeability, Inertial Loss Coefficients and Porosity

The empirical correlation of the Ergun equation (Eq. (13)) is applicable over a wide range of Reynolds numbers and many types of packed beds (Ergun, 1952).

$$\frac{-\Delta P_c}{L_c} = 150\mu\frac{(1-\varepsilon)^2}{\varepsilon^3}\frac{V}{d_p^2} + 1.75\rho\frac{(1-\varepsilon)}{\varepsilon^3}\frac{V^2}{d_p} \tag{13}$$

From the Ergun correlation, the permeability α and inertial loss coefficients (Inertial resistance) C_2 are obtained as follows:

$$\alpha = \frac{d_p^2}{150}\frac{\varepsilon^3}{(1-\varepsilon)^2} \tag{14}$$

$$C_2 = \frac{3.5}{d_p}\frac{(1-\varepsilon)}{\varepsilon^3} \tag{15}$$

A standard correlation for predicting the total porosity ε of a catalyst-packed bed consisting of random spherical particles of similar size was developed by Dixon (1988), Theuerkauf et al. (2006), and is given as:

$$\varepsilon = 0.4 + 0.05\frac{d_p}{D_C} + 0.412\left(\frac{d_p}{D_C}\right)^2 \tag{16}$$

4. METHODOLOGY OF RESOLUTION

4.1 Grid Independent Study

The mesh was generated using a uniform quadrilateral grid. To reduce the number of elements and significantly save computational cost, an axis-symmetric (half geometry) approach was used, as shown in Fig. 3. Table 3 presents the parameters of the grid independence study and shows that the maximum temperatures recorded in the catalyst bed were 968K for Mesh 1 and

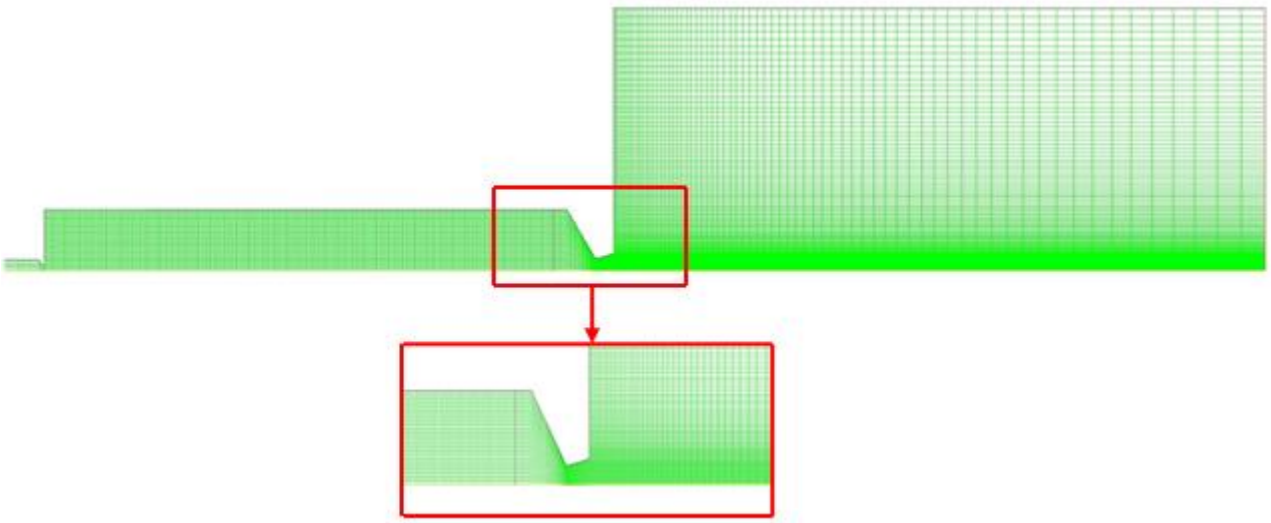

Fig. 3 2D model of axis-symmetric mesh geometry (half geometry) with quadrilateral grid

Table 3 Grid independent study

Meshes	Number of nodes	Number of elements	Maximum Temperature at catalyst bed [K]
Mesh 1	17648	17045	968
Mesh 2	18534	17913	968
Mesh 3	22518	21822	980

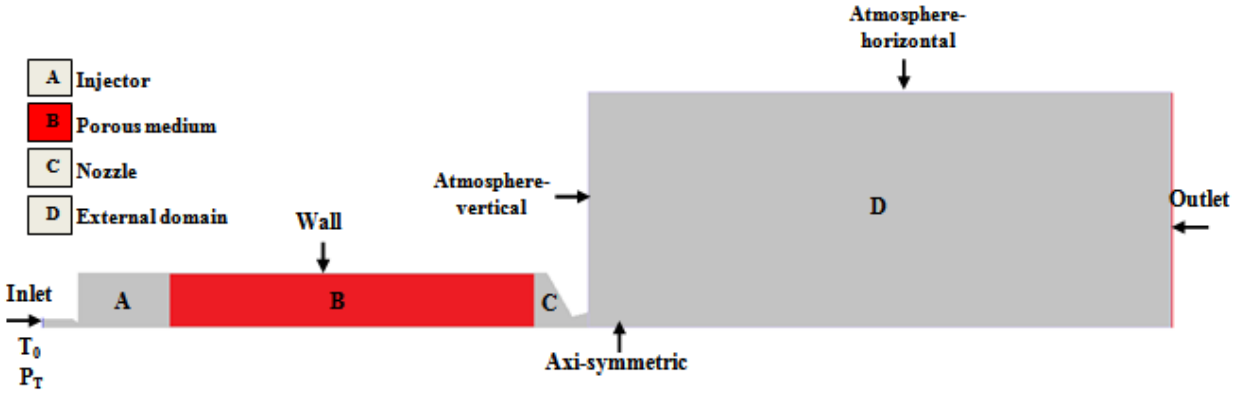

Fig. 4 Boundary conditions and cell zone conditions of the 2D model

Mesh 2 and 980K for Mesh 3. This indicates that there were no significant temperature differences between Mesh 1 and Mesh 2. Mesh 1 was selected for this study to minimize computational cost with a total of 17648 nodes and 17045 elements, based on the results of the preliminary mesh convergence study.

4.2 Setup Procedure

The analysis of the two-dimensional monopropellant thruster was carried out using a computational fluid dynamics (CFD) model in ANSYS Fluent software to study the flow of hydrogen peroxide within the thruster. The simulation was conducted as a steady-state analysis using a pressure-based solver with an axis-symmetric geometry. The energy equation is employed to calculate thermal effects. To model turbulent flow, the k-ω turbulence model of shear-stress transport (SST) was selected (Menter, 1994), which is used to simulate supersonic flow (Jayakrishnan & Deepu, 2020). The model combines the standard k-ω and k-ε models, with the k-ω model functioning in the near-wall region and the k-ε model being active in the far field (Jones & Launder, 1973; Wilcox, 1998). This method is particularly effective for free flow away from the wall and is well suited for flow separation, as it accounts for the transfer of turbulent shear stress. To ensure the continuity of the velocity vectors through the interface of the porous medium, we adopted a superficial velocity approach computed based on the volumetric flow rate. We used the species transport option to model the hydrogen peroxide decomposition reaction, considering that the reaction occurs only within the catalyst bed. In turbulent chemical interactions, we used the eddy dissipation model (EDM). As for boundary conditions, we treated all walls as adiabatic with no heat flux and no-slip conditions. The inlet pressure of the fluid was set to 17bar, with a temperature of 293.15K for hydrogen peroxide. The mass fractions of H_2O_2 and H_2O were set to 0.875 and 0.125, respectively, with a mass molar of 22g/mol. The outlet pressure is set to 0bar. The catalyst bed region was modelled as a porous medium, as shown in Fig. 4, and the source terms for the local thermal non-equilibrium (LTNE) model were computed using a user-

Table 4 The data used in the simulation

Parameter	Value
Porosity ε	0.4019
Viscous resistance $1/\alpha$	1.9554×10^{9} m^{-2}
Inertial resistance C_2	5520.5 m^{-1}
Inlet absolute pressure P_T	17 bar
Inlet temperature T_0	293.15 K
Concentration of H_2O_2	87.5 %
Operating pressure P	1.1325

defined function (UDF) to relate the energy equations of the fluid and solid phases.

In the solution methods, a coupled scheme was applied, and we used the second-order upwind method for the advection terms in the momentum and energy equations. A hybrid initialization approach was utilized for this model, with a convergence criterion set at 10^{-5} for all equations within the model. Figure 4 presents the boundary conditions for the analysed problem. The analysis was performed for H_2O_2 flow to determine the thermal behaviour of the catalyst bed (porous medium), and chemical reactions were included in the model to analyse the kinetics of the reactions and their effect on the thermal behaviour of the thruster.

5. RESULTS AND DISCUSSION

5.1 Validation Process

To validate the developed model, a benchmark analysis was performed using numerical and experimental results obtained from Muhammad et al. (2021) and Palmer (2014). As shown in Fig. 5, the results indicate excellent agreement with the experimental results, with a maximum error of the temperature in the thruster of less than 1%. Furthermore, the numerical results showed that the maximum error does not exceed 6%.

5.2 Thermodynamic Parameter Analysis of the Thruster Based on Catalyst Bed Made of Spherical Silver Particles

To optimize the performance of the catalytic bed, uniformly sized spherical silver particles were used as a porous medium for hydrogen peroxide decomposition, yielding a calculated porosity of 0.4019 based on the Dixon equation (Dixon, 1988). Figure 5 illustrates the temperature variation along the length of the thruster, with an external domain showing the flow after the nozzle.

The static temperature increases from the catalyst bed to the nozzle exit, reaching 968K, as illustrated in Fig. 6. The flow carries the heat from the reaction as a hot gas through the nozzle, transitioning into supersonic flow after passing through the nozzle throat. In contrast, the temperature of the compressible gas remains constant at the stagnation temperature of the fluid flow. Within the nozzle region, the stagnation temperature remains constant according to the principles of supersonic nozzle flow (White, 2006). The heat flux outside the thruster then begins to decrease as the distance from the reaction site increases.

The high decomposition temperature of hydrogen peroxide plays an important role in ensuring the high performance of propulsion systems. This is due to two main factors: using a high concentration of hydrogen peroxide and selecting the appropriate catalyst bed. Hydrogen peroxide decomposes within the catalyst bed, producing oxygen gas and water vapor. Figure 7 illustrates the variation in H_2O_2, H_2O, and O_2 mass fractions along the thruster length. H_2O_2 enters with a mass flow rate of 0.875 and decreases significantly as it reaches the catalyst bed. This indicates the occurrence of

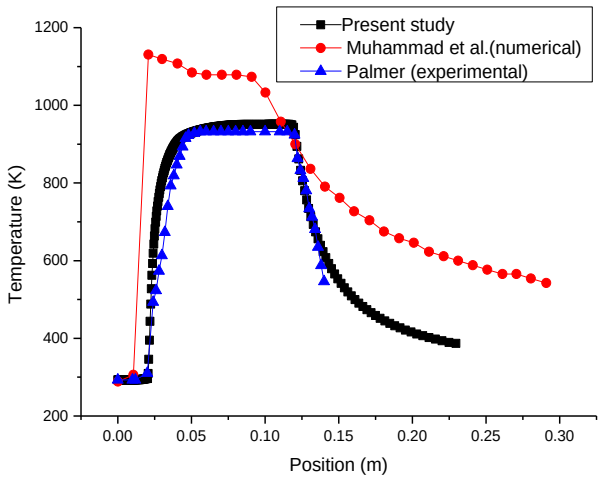

Fig. 5 Temperature distribution for Muhammad et al. (2021), palmer (2014) and current numerical simulation

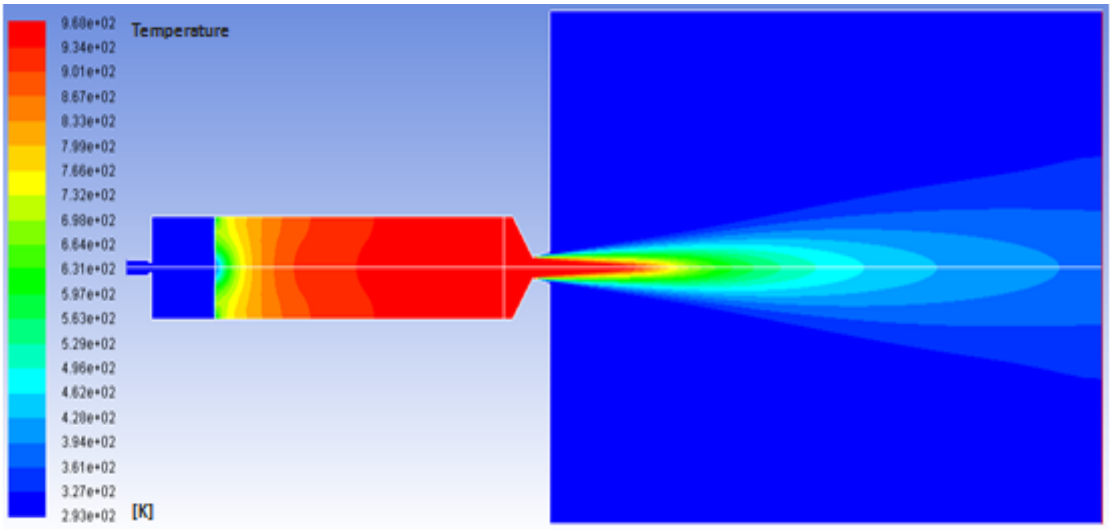

Fig. 6 Static temperature contour across the thruster

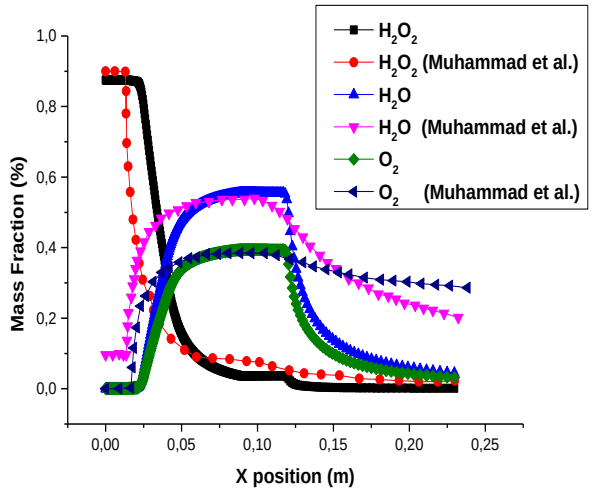

Fig. 7 Species mass fraction across thruster for Muhammad et al. (2021) and current numerical simulation

a reaction that leads to the formation of oxygen gas and water vapor and an increase in their mass fraction. As depicted in Fig. 8, the mass fraction of H_2O_2 continuously decreases as H_2O_2 is replaced by H_2O and O_2 until they both reach their maximum stoichiometric mass fraction values of 0.580 and 0.412, respectively.

The analysis of the graph of species mass fractions (Fig. 7) along the temperature contour (Fig. 6) shows that the flow undergoes the correct decomposition reaction, with heat generated by the reaction. This observation confirms the reliability of the simulation results.

Figure 10 presents the velocity behaviour across the thruster. The velocity increases in the injector and divergent nozzle region, except in the catalyst bed region, where it remains uniform. This uniformity of the catalyst bed velocity is assumed to ensure flow continuity expressed by an isotropic catalyst bed. The velocity decreases significantly in the catalyst bed region, reaching around 58.4m/s, when the fluid contacts the porous medium. The convergent-divergent (CD) profile of the nozzle accelerates the gas flow from subsonic to supersonic velocity. As shown in Fig. 9, the velocity of the divergent part increases gradually and reaches a maximum value of 1.17×10^3m/s at the nozzle exit. These results are consistent with the theory of supersonic convergent-divergent nozzles (White, 2006). Consequently, the results confirmed the possibility of achieving a thrust force of 20N (17×10^{-3}kg/s $\times1.17\times10^3$m/s) required for this study and a specific impulse of about 120s as calculated from Eqs. (17) and (18), respectively.

$$\dot{m} = \frac{F_T}{V_e} \tag{17}$$

$$I_{sp} = \frac{V_e}{g} \tag{18}$$

5.3. Effect of Particle Diameter of the Catalyst Bed on the Thruster Performance

In this section, we will conduct an extensive analysis of the catalyst bed, focusing on spherical silver particles with varying diameters. The objective is to explore how these variations affect the decomposition phenomena, the exit velocity, and the required thrust force.

The temperature within the catalyst bed exhibits a direct correlation with the diameter of the spherical particles. As the diameter increases, so does the temperature, culminating in a peak temperature of 994K at a diameter of 1.2mm. Figure 11 illustrates the relationship between temperature and varying diameter values.

Additionally, the velocity measured at the nozzle exit demonstrates behaviour analogous to that of the temperature. Specifically, as the diameter of the spherical particles increases, the velocity increases almost linearly. This phenomenon leads to a corresponding increase in thrust force, as depicted in Fig. 11, with the thrust force rising from 17N to 22N.

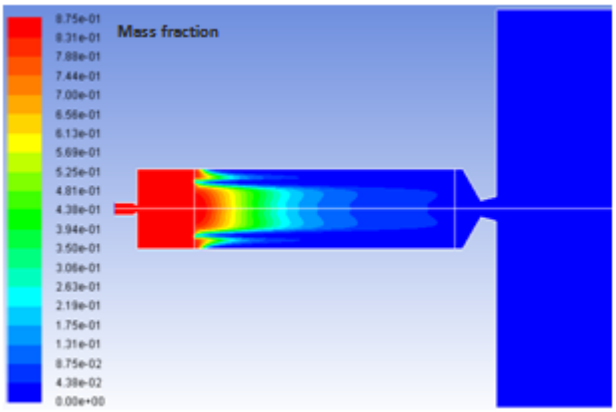

(a) H_2O_2

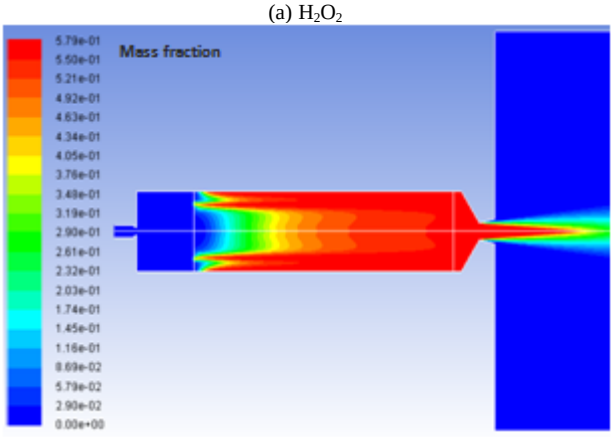

(b) H_2O

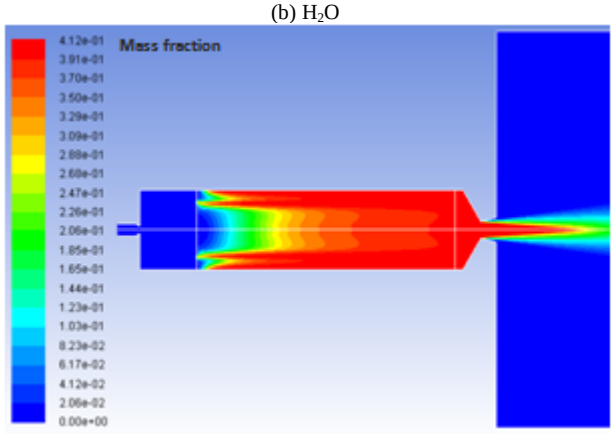

(c) O_2

Fig. 8 Species mass fraction contours across thruster

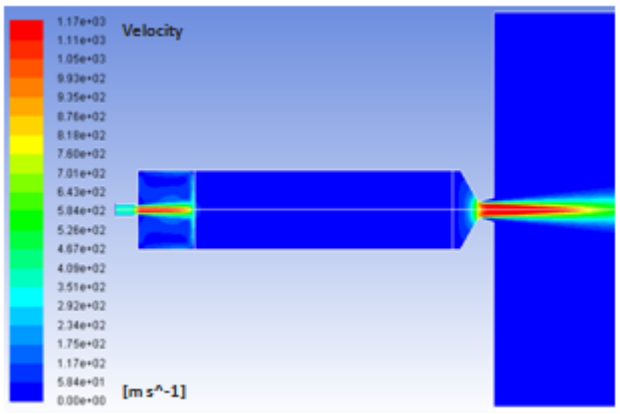

Fig. 9 Velocity magnitude contour across the thruster

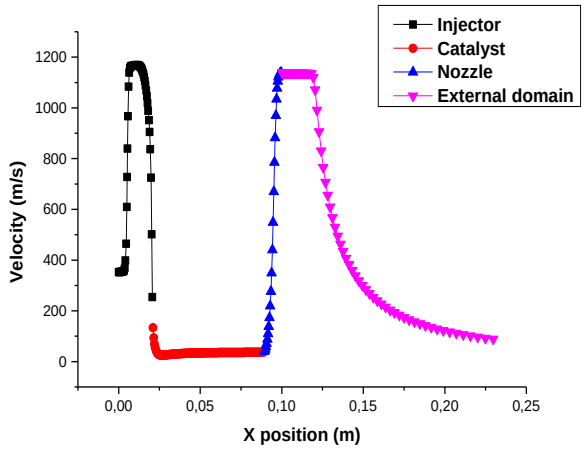

Fig. 10 Velocity magnitude distribution

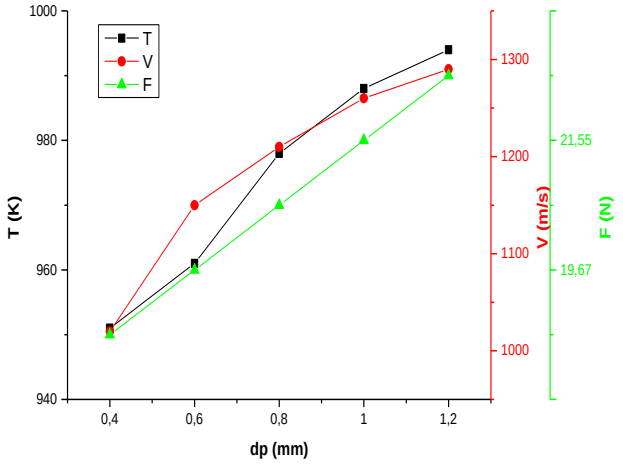

Fig. 11 Graphs of catalyst bed temperature, exit velocity, and thrust force according to spherical silver particles diameter of the catalyst bed

As a result, 0.65mm is the optimal diameter for achieving maximum performance in terms of temperature, exit velocity, and the required thrust force of 20N.

6. CONCLUSION

In the current paper, through a detailed analysis of the diameters of the particles comprising the porous catalyst bed, we conducted both analytical and numerical studies to optimize the design of a monopropellant thruster capable of generating a thrust of 20N.

The study on temperature behaviour was carried out using the local thermal non-equilibrium (LTNE) model. A numerical study was conducted to analyse thermal reactions, species mass fractions, and exit velocities. The simulations were validated and compared with experimental and numerical data.

The porous medium significantly affects the propellant decomposition within the thruster. Regarding

the reactive flow simulation, the effect of the reaction on the temperature distributions was analysed, revealing an increase in temperature to about 968K due to the exothermic reaction, which was sufficient for the decomposition of hydrogen peroxide. The results showed that the catalyst bed gives an optimal decomposition of H_2O_2.

To scrutinize the influence of the diameter of the spherical silver particles and determine the most optimal value, a dedicated simulation was performed. The simulation encompassed a range of diameter values ranging from 0.4 to 1.2mm. The results of the simulation confirm that the optimal decomposition of H_2O_2 involves using spherical silver particles with a diameter of 0.65mm. This configuration exhibits superior performance in various critical parameters, including reaction temperature, exit velocity, and the required thrust force of 20N with a specific impulse of about 120s.

From a broader perspective, it is advisable to investigate alternative flow configurations within catalyst beds in which the spherical particles are made from various materials and come in different sizes, thus ensuring variable porosity within the catalyst. Such an approach could increase the effectiveness of monopropellant thrusters for propulsion systems using green propellants.

ACKNOWLEDGEMENTS

This study is part of the research proposed in the Laboratory of Applied Thermal Energy (ETAP), Department of Mechanical Engineering at the University of Technology in Tlemcen, Algeria. We appreciate and recognize everyone for their help and efforts in this work.

CONFLICT OF INTEREST

The author declared that they have no competing interests.

AUTHORS CONTRIBUTION

F. Benzenine: the design and simulation, writing the manuscript and contributing to answering comments. **C. Seladji:** supervision; review and editing. **D. Darfilal:** supervision; review, editing and contributing to answering comments. **O. Bendermel:** supervision; contributed to design and simulation.

REFERENCES

Abdedou, A., & Bouhadef, K. (2015). Comparison between Two Local Thermal Non Equilibrium Criteria in Forced Convection through a Porous Channel. *Journal of Applied Fluid Mechanics*, *8*(3), 491-498. http://dx.doi.org/10.18869/acadpub.jafm.67.222.22233

Achenbach, E. (1995). Heat and flow characteristics of packed beds. *Experimental Thermal and Fluid Science*, *10*, 17-27. https://doi.org/10.1016/B978-0-444-816191.50029-0

Adami, A., Mortazavi, M., & Nosratollahi, M. (2015). Multidisciplinary design optimization of hydrogen peroxide monopropellant propulsion system using GA and SQP. *International Journal of Computer Applications*, *113*(9), 14–21. http://doi.org/10.5120/19853-1774

Alazmi, B., & Vafai, K. (2000). Analysis of variants within the porous media transport models. *Journal of Heat Transfer*, *122*(2), 303-326. https://doi.org/10.1115/1.521468

Amiri, A., & Vafai, K. (1994). Analysis of dispersion effects and non-thermal equilibrium, non-darcian, variable porosity incompressible flow through porous media. *International Journal of Heat and Mass Transfer*, *37*, 939-54. https://doi.org/10.1016/0017-9310%2894%2990219-4

Amiri, A., Vafai, K., & Kuzay, T. M. (1995). Effects of boundary conditions on non-darcian heat transfer through porous media and experimental comparisons. *Numerical Heat Transfer*, *27*, 651-64. https://doi.org/10.1080/10407789508913724

Amri, R., Gibbon, D., & Rezoug, T. (2013). The design, development and test of one newton hydrogen peroxide monopropellant thruster. *Aerospace Science and Technology*, *25*(1), 266-272. https://doi.org/10.1016/j.ast.2012.02.002

An, S., & Kwon, S. (2009). Scaling and evaluation of pt/al2o3 catalytic reactor for hydrogen peroxide monopropellant thruster. *Journal of Propulsion and Power*, *25*(5), 1041-1045. http://dx.doi.org/10.2514/1.40822

An, S., Jin, J., Lee, J., Jo, S., Park, D., & Kwon, S. (2010). Chugging instability of H_2O_2 monopropellant thrusters with reactor aspect ratio and pressures. *Journal of Propulsion and Power*, *27*(2), 422–427. http://dx.doi.org/10.2514/1.48939

Cervone, A., Torre, L., d'Agostino, L., Musker, A. J., Roberts, G. T., Bramanti, C., & Saccoccia, G. (2006, July). *Development* of Hydrogen Peroxide Monopropellant Rockets. 42nd AIAA/ASME/SAE/ASEE Joint Propulsion Conference & Exhibit, Joint Propulsion Conferences. https://doi.org/10.2514/6.2006-5239

Chan, Y., Liu, H., Tseng, K., & Kuo, T. (2013). Preliminary development of a hydrogen peroxide thruster. *International Journal of Aerospace and Mechanical Engineering*, *7*(7), 1546-1553. https://doi.org/10.5281/zenodo.1087287

Coxhill, I. (2002). *An investigation of a low cost Bi-Propellant rocket engine for small satellites*. [PhD. thesis, Surrey Space Centre School of Electronics and Physical Sciences, University of Surrey]. United Kingdom.

Dixon, A. G. (1988). Correlations for wall and particle shape effects on fixed bed bulk voidage. *The Canadian Journal of Chemical Engineering*, *66*, 705–708. https://doi.org/10.1002/cjce.5450660501

Dixon, A. G., & Cresswell, D. L. (1979). Theoretical prediction of active heat transfer parameters in packed beds. *AIChE Journal*, *25*, 663-76. https://doi.org/10.1002/AIC.690250413

Ergun, S. (1952). Fluid flow through packed columns. *Chemical Engineering Progress*, *48*, 89–94. https://books.google.dz/books/about/Fluid_Flow_Through_Packed_Columns.html?id=37sgywEACAAJ&redir_esc=y

George, P. S. (2003). History of liquid-propellant rocket engines in russia, formerly the soviet union. *Journal of Propultion and Power*, *19*(6). https://doi.org/10.2514/2.6943

Gibbon, D., Paul, M., Jolley, P., Zakirov, V., Haag, G., Coxhill, I., Sweeting, M., & Eloirdi, R. (2001). Energetic green propulsion for small spacecraft. *AIAA*, 2001-3247. https://doi.org/10.2514/6.2001-3247

Haq, N. U., Khan, R. A., & Mehmood, R. (2017). *Design, development and testing of 1N Hydrogen Peroxide thruster*. 14th International Bhurban Conference on Applied Sciences and Technology (IBCAST) IEEE, 599-607. https://doi.org/10.1109/IBCAST.2017.7868112

Hwang, C. H., Lee, S., Baek, S, Han, C. Y., Kim, S. K., & Yu, M. J. (2012). Effects of catalyst bed failure on thermochemical phenomena for a hydrazine monopropellant thruster using Ir/Al2O3 catalysts. *Industrial & Engineering Chemistry Research*, *51*(15), 5382−5393. https://doi.org/10.1021/ie202347f

Hwang, G. J., Wu, C. C., & Chao, C. H. (1995). Investigation of non-darcian forced convection in an asymmetrically heated sintered porous channel. *J Heat Transfer*, *117*(3), 725-732. https://doi.org/10.1115/1.2822636

Jayakrishnan, S., & Deepu, M. (2020). Reacting flow Simulations of a Dual Throat-Dual Fuel Thruster. *Journal of Applied Fluid Mechanics*, *14*(1), 49-59. https://doi.org/10.47176/jafm.14.01.31329

Jones, W., & Launder, B. (1973). The calculation of low-Reynolds-number phenomena with a two equation model of turbulence. *International Journal of Heat and Mass Transfer*, *16*(6), 1119-1130. https://doi.org/10.1016/00179310(73)90125-7

Koopmans, R. J., Shrimpton, J. S., Robert, G. T., & Musker, A. J. (2014). Dependence of pellet shape and size on pressure drop in H_2O_2 thrusters. *Journal of Propulsion and Power*, *30*(3), 775–789. http://dx.doi.org/10.2514/1.B35072

Kouichi, K. (2008). Modeling of composite heat transfer in open-cellular porous materials at hight temperatures. In Book: Cellular and Porous Materials: *Thermal Properties Simulation and Prediction*, 165-198. https://doi.org/10.1002/9783527621408.ch6

Krejci, D., Woschnak, A., Scharlemann, C., & Ponweirser, K. (2011). Hydrogen peroxide decomposition for micro propulsion: Simulation and experimental verification. *47th AIAA/ASME/SAE/ASEE Joint Propulsion Conference & Exhibit*, 5855. https://doi.org/10.2514/6.2011-5855

Kuan, C. K., Chen, G. B., & Chao, Y. C. (2007). Development and ground tests of a 100-millinewton hydrogen peroxide monopropellant microthruster. *Journal of Propulsion and Power*, *23*(6), 1313-1320. https://doi.org/10.2514/1.30440

Lee, S. L., & Lee, C. (2009). Performance characteristics of silver catalyst bed for hydrogen peroxide. *Aerospace Science and Technology*, *13*(1), 12-17. https://doi.org/10.1016/j.ast.2008.02.007

Menter, F. R. (1994). Two-equation eddy-viscosity turbulence models for engineering applications. *AIAA Journal*, *32*(8), 1598–1605. https://doi.org/10.2514/3.12149

Morlan, P., Wu, P., Nejad, A., Ruttle, D., & Fuller, F, (1999). Catalyst development for hydrogen peroxide rocket engines. *AIAA*, 1999-2740. https://doi.org/10.2514/6.1999-2740

Muhammad, S. S. N., Othman, N., Ahmad, N., Mohd, R. N., Wahid, M. A., & Zarhamdy, M. M. Z. (2021). Porosity effect of the silver catalyst in hydrogen peroxide monopropellant thruster. *Journal of CFD Letters*, *13*(12), 1-20. https://doi.org/10.37934/cfdl.13.12.120

Musker, A. J., Rusek, J. J., Kappenstein, G. T., & Roberts, C. (2006, September). *Hydrogen peroxide-from bridesmaid to bride for space propulsion.* Proc. of the 3rd International Conference on Green Propellants, Poitiers, France. http://eprints.soton.ac.uk/id/eprint/43655

Palmer, M. J. (2014). Experimental evaluation of hydrogen peroxide catalysts for monopropellant attitude control thrusters [PhD. thesis, University of Southampton]. Faculty of Engineering and the Environment, United Kingdom. http://eprints.soton.ac.uk/id/eprint/385352

Pasini, A., Torre, L., Romeo, L., Cervone, A., & d'Agostino, L. (2008). Testing and characterization of a hydrogen peroxide monopropellant thruster. *Journal of Propulsion and Power*, *24*(3), 507–515. http://dx.doi.org/10.2514/1.33121

Pędziwiatr, P., Mikołajczyk, F., Zawadzki, D., Mikołajczyk, K., & Bedka, A. (2018). Decomposition of hydrogen peroxide-kinetics and review of chosen catalysts. *Acta Innovations*, *26*(5), 45-52. https://doi.org/10.32933/ACTAINNOVATIONS.26.5

Runckel, J. F., Willis, C. M., & Salters, L. B. (1963). *Investigation of catalyst beds for 98-percent-concentration hydrogen peroxide*. NASA TN D-1808, Washington.

Rusek, J. J. (1996). New decomposition catalysts and characterization techniques for rocket-grade hydrogen peroxide. *Journal of Propulsion and Power*, *12*(3), 574–580. https://doi.org/10.2514/3.24071

Ryan, C. N., Fonda, M. E., & Roberts, G. (2020). Experimental validation of a 1 newton hydrogen peroxide thruster. *Journal of Propulsion and Power*, *36*(2). 1-9. http://dx.doi.org/10.2514/1.B37418

Sippel, T., Shark. S., Hinkelman, M., & Heister, S. (2011). *Hypergolic ignition of metal hydride-based fuels with hydrogen peroxide.* 7th US National Combustion Meeting, Atlanta. https://www.researchgate.net/publication/265727021

Soejima, M., Nojim, K., Tomioka, S., & Sakuranaka, N. (2016). Development of the fuel heating device for the component test of aerospace propulsion systems, *Journal of Fluid Science and Technology*, *11*(1), 1-10. https://doi.org/10.1299/jfst.2016jf

Srivastava, A. K., & Bhadauria, B. S. (2016). Influence of magnetic field on fingering instability in a porous medium with cross-diffusion effect: a thermal non-equilibrium approach. *Journal of Applied Fluid Mechanics*, *9*(6), 2845-2853. http://dx.doi.org/10.29252/jafm.09.06.25977

Theuerkauf, J., Witt, P., & Schwesig, D. (2006). Analysis of particle porosity distribution in fixed beds using the discrete element method. *Powder Technology*, *165*(2), 92–99. https://doi.org/10.1016/j.powtec.2006.03.022

Vafai, K., & Amiri, A. (1998). Non-Darcian effects in confined forced convective flows. *Transport Phenomena in Porous Media*, 1, 313-329. https://doi.org/10.1016/b978-008042843-7/50013-1

Ventura, M., & Wernimont, E. (2001, July). *Advancements in high concentration hydrogen peroxide catalyst beds.* 37th AIAA/ASME/SAE/ASEE, Joint Propulsion Conference, Salt Lake City, Utah. https://doi.org/10.2514/6.2001-3250

Vestnes, F. (2016). *A CFD-model of the fluid flow in a hydrogen peroxide monopropellant rocket engine in ANSYS fluent 16.2* [Master's thesis, University of Science and Technology Norwegian]. http://hdl.handle.net/11250/2408892

Villafán, V. H., Stéphane, A., Cyril, C., & Romero, P. H. (2011). Heat transfer simulation in a thermochemical solar reactor based on a volumetric porous receiver. *Applied Thermal Engineering*, *31*(16), 3377-3386. https://doi.org/10.1016/j.applthermaleng.2011.06.022

Walter, H. (1956). Hydrogen Peroxide Rockets. In T. Benecke & A. W. Quick (Eds.), *History of german guided missile developments, AGARDo graph*,Vol. 20, Butter worths, London.

White, F. M. (2006). *Fluid Mechanics, McGraw-Hill*. 7th edition, New York, USA.

Wilcox, D. C. (1998). *Turbulence modeling for CFD.* Second Edition, D.C.W. Industries.

Xu, C., Song, Z., & Zhen, Y. (2011). Numerical investigation on porous media heat transfer in a solar tower receiver. *Renewable Energy*, *36*(3), 1138-1144. https://doi.org/10.1016/j.renene.2010.09.017

Xue, L., Guo, X., & Chen, H. (2020). Fluid Flow in Porous Media. Chapter 2: Basic theory. World Scientific, p 408. https://doi.org/10.1142/11805